THEMIS Spacecraft Multi-Body Stability Analysis

Richard L. LeBoeuf
Swales Aerospace & University of South Carolina Upstate
University of South Carolina Upstate
800 University Way
Spartanburg, SC 29303; (864) 640-1147
rleboeuf@uscupstate.edu

ABSTRACT

Stability criteria for a spinning multi-body spacecraft were derived and applied to the THEMIS spacecraft. This paper will discuss a number of aspects of the stability analysis developed and implemented by Swales Aerospace, the spacecraft bus provider. The derivation accommodates a non-axisymmetric central body and arbitrary axial and radial boom locations. Stability criteria expressed in terms of effective inertias, were derived by maximizing the spin axis inertia. Essential details of the derivation and unique plots illustrating the stability criteria were included in this paper. A multi-body time-domain simulation developed to verify dynamic behavior of the THEMIS spacecraft was used to validate the stability criteria for a large number of deployment states. The derived stability criteria capture the affects of the central body, the stabilizing influence of the flexible radial booms, and the destabilizing influence of the flexible axial booms. They were used to determine the optimum lengths of the axial and radial booms given central body mass properties. The stability criteria presented in this paper can be readily applied to other axisymmetric or non-axisymmetric spinning spacecraft with axial and radial booms to ensure sufficient stability margins exist for all deployment configurations.

INTRODUCTION

The THEMIS project, a NASA Medium-Class Explorer (MIDEX) mission, managed by the University of California at Berkeley and launched in February 2007, was the first NASA mission to launch five science satellites simultaneously. The probes were spin stabilized spacecraft with 8 deployable instruments which drove the stability analysis.

For stable spin of a rigid body, the spin axis inertia must be greater than the transverse inertias. The ratio of spin-axis inertia to transverse axis inertia relative to a value of 1 provides an indication of the degree of stability. Similar criteria, using "effective inertias," apply to spacecraft with flexible appendages. The effective inertia ratio must be greater than 1 to ensure stability of a spinning spacecraft. The derivation presented herein develops effective inertias that account for central body and appendage inertia contributions.

A large body of research in the 1960's and 1970's was devoted to developing stability criteria for spinning flexible spacecraft using energy considerations and Liapunov analysis. To obtain literal closed-form stability criteria, these methods were applied to idealized configurations not representative of the THEMIS configuration. For example, Crist and Eisley[1] treated the elastic dumbbell configuration. Meirovitch[2] analyzed flexible antennas projected along the spin axis. Barbera & Likins[3] assumed a model with a planar appendage in a spin plane located at the center of mass. Meirovitch and Calico[4,5] treated the problem of a central body with flexible appendages emanating along the central body principal axes. Whereas THEMIS probes have radial booms mounted roughly 45 degrees from the central body principle axes. Meirovitch and Nelson[6], Meirovitch[7], and Dong & Schlack[8] treated the configuration with spin-axis antennas, which is a subset of the THEMIS configuration. Limp radial wire booms, features of THEMIS and some other spacecraft, were not explicitly considered by these references.

The derivation herein is an extension of an unpublished inertia-based derivation of stability criteria in terms of effective inertias by Pankow for axisymmetric central body rotation with flexible axial booms and limp radial wire booms*. The extensions include unequal central body transverse inertias, non-zero central body products of inertia, offset of the radial booms from the center of mass axial location, and arbitrary rotation of the central body tilt direction.

* Pankow, D.H., "SMEX/FAST Spin Axis Spin Stability Discussion and Review"

STABILITY CRITERIA

Stability criteria were derived for a general rigid central body with radial appendages having freely rotating joint at the central body attachment point and flexible axial appendages (Figure 1). The derivation considers the contribution of each spacecraft component to the spin axis inertia. The process involves differentiating spin axis inertia contributions with respect to central body tilt angles. For the configuration to be a stable maximum inertia axis spinner, the first partial derivatives must be equal to zero and the second partial derivatives must be negative for zero tilt angles.

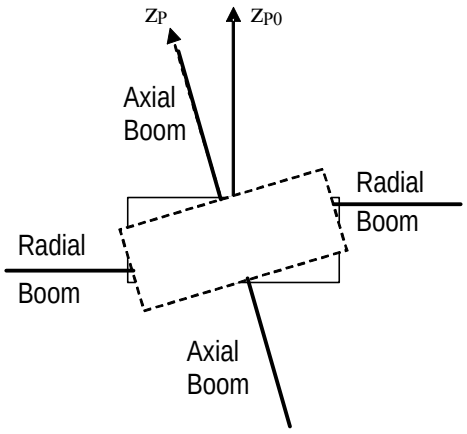

Figure 1: Nominal and Perturbed Orientations

Central Body Contributions

The perturbed spacecraft (probe) frame (*P*) is rotated via a 1-2 rotation sequence relative to the nominal probe frame (P_0) (Figure 2). For spin about the central body Z-axis, $\alpha = 0$ and $\beta = 0$.

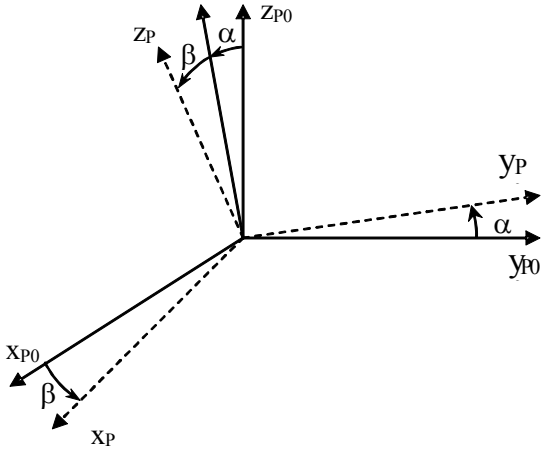

Figure 2: Nominal and Perturbed Frames

Therefore, the transformation from the nominal to the perturbed probe frame is

$$C_{P_0}^{P} = \begin{bmatrix} \cos\beta & \sin\beta\sin\alpha & -\sin\beta\cos\alpha \\ 0 & \cos\alpha & \sin\alpha \\ \sin\beta & -\cos\beta\sin\alpha & \cos\beta\cos\alpha \end{bmatrix} \quad (1)$$

where

α is the rotation angle of the central body from the P_0 frame to the P frame about the X axis (axis 1)

β is the rotation angle of the central body from the P_0 frame to the P frame about the intermediate Y axis (axis 2)

The central body moment of inertia (MOI) about the nominal frame, given the inertia with respect to perturbed frame axes, I^P , is

$$I^{P_0} = \left[C_{P_0}^{P}\right]^T I^P C_{P_0}^{P} = \begin{bmatrix} * & * & * \\ * & * & * \\ * & * & I_{ZZ0,cb} \end{bmatrix} \quad (2)$$

where $*$ represents terms irrelevant to this derivation and the central body contribution to the Z-axis inertia, $I_{zz0,cb}$, is

$$\begin{aligned} I_{zz0,cb} = {} & I_{xx}^{P}\sin^2\beta\cos^2\alpha + I_{yy}^{P}\sin^2\alpha \\ & + I_{zz}^{P}\cos^2\beta\cos^2\alpha - I_{xy}^{P}\sin\beta\sin 2\alpha \\ & - I_{xz}^{P}\sin 2\beta\cos^2\alpha + I_{yz}^{P}\cos\beta\sin 2\alpha \end{aligned} \quad (3)$$

An example of the central body spin axis inertia as a function of α and β is depicted in Figure 3. The central body in this example has a stabilizing influence for spin about the Z-axis. The first partial derivatives with respect to α and β would be zero and the second partial derivatives would be negative indicating the central body inertia is maximum for α = 0 and β = 0.

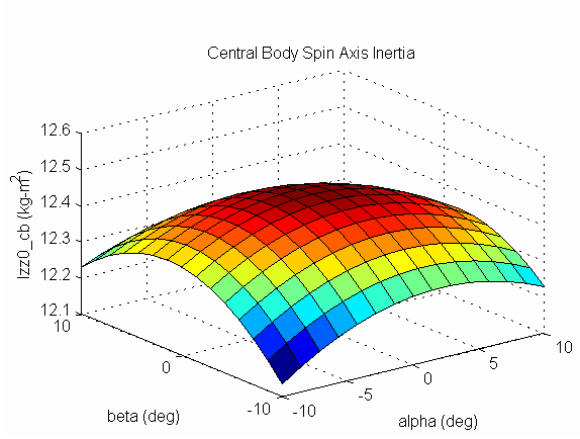

Figure 3: Central Body Spin Axis Inertia Example

Taking first partial derivatives of Eq. (3) yields

$$\begin{aligned}\frac{\partial I_{zz0,cb}}{\partial \alpha} &= -I_{xx}^{P}\sin^2\beta\sin 2\alpha + I_{yy}^{P}\sin 2\alpha \\ &\quad - I_{zz}^{P}\cos^2\beta\sin 2\alpha - 2I_{xy}^{P}\sin\beta\cos 2\alpha \\ &\quad + I_{xz}^{P}\sin 2\beta\sin 2\alpha + 2I_{yz}^{P}\cos\beta\cos 2\alpha\end{aligned} \tag{4a}$$

$$\begin{aligned}\frac{\partial I_{zz0,cb}}{\partial \beta} &= I_{xx}^{P}\sin 2\beta\cos^2\alpha - I_{zz}^{P}\sin 2\beta\cos^2\alpha \\ &\quad - I_{xy}^{P}\cos\beta\sin 2\alpha - 2I_{xz}^{P}\cos 2\beta\cos^2\alpha \\ &\quad - I_{yz}^{P}\sin\beta\sin 2\alpha\end{aligned} \tag{4b}$$

For $\alpha = 0$ and $\beta = 0$, Eq. (4) becomes

$$\left.\frac{\partial I_{zz0,cb}}{\partial \alpha}\right|_{\alpha=0,\beta=0} = 2I_{yz}^{P} \tag{5a}$$

$$\left.\frac{\partial I_{zz0,cb}}{\partial \beta}\right|_{\alpha=0,\beta=0} = -2I_{xz}^{P} \tag{5b}$$

A single rigid body must have no principal axis offset to be a stable spinner about its Z-axis.

Taking second partial derivatives of Eq. (3) yields

$$\begin{aligned}\frac{\partial^2 I_{zz0,cb}}{\partial \alpha^2} &= -2I_{xx}^{P}\sin^2\beta\cos 2\alpha + 2I_{yy}^{P}\cos 2\alpha \\ &\quad - 2I_{zz}^{P}\cos^2\beta\cos 2\alpha + 4I_{xy}^{P}\sin\beta\sin 2\alpha \\ &\quad + 2I_{xz}^{P}\sin 2\beta\cos 2\alpha - 4I_{yz}^{P}\cos\beta\sin 2\alpha\end{aligned} \tag{6a}$$

$$\begin{aligned}\frac{\partial^2 I_{zz0,cb}}{\partial \beta^2} &= 2I_{xx}^{P}\cos 2\beta\cos^2\alpha - 2I_{zz}^{P}\cos 2\beta\cos^2\alpha \\ &\quad + I_{xy}^{P}\sin\beta\sin 2\alpha + 4I_{xz}^{P}\sin 2\beta\cos^2\alpha \\ &\quad - I_{yz}^{P}\cos\beta\sin 2\alpha\end{aligned} \tag{6b}$$

For $\alpha = 0$ and $\beta = 0$ Eq. (6) becomes

$$\left.\frac{\partial^2 I_{zz0,cb}}{\partial \alpha^2}\right|_{\alpha=0,\beta=0} = 2I_{yy}^{P} - 2I_{zz}^{P} = 2\left(I_{yy}^{P} - I_{zz}^{P}\right) \tag{7a}$$

$$\left.\frac{\partial^2 I_{zz0,cb}}{\partial \beta^2}\right|_{\alpha=0,\beta=0} = 2I_{xx}^{P} - 2I_{zz}^{P} = 2\left(I_{xx}^{P} - I_{zz}^{P}\right) \tag{7b}$$

Central body results were combined with radial and axial boom results in a later section.

Radial Booms

For the purpose of this analysis, the radial booms have no bending stiffness, so spin induced centripetal acceleration causes them to travel in a plane normal to the spin vector. The radial booms were modeled as point masses connected to the central body by massless rods. The vector from the probe center of mass to the radial boom connection (hinge point, *hp*) on the perturbed central body expressed in nominal probe frame (P_0) coordinates, $\vec{r}_{cm\to hp}^{\,P_0}$, is

$$\vec{r}_{cm\to hp}^{\,P_0} = \begin{bmatrix} x_{cm\to hp}^{P_0} \\ y_{cm\to hp}^{P_0} \\ z_{cm\to hp}^{P_0} \end{bmatrix} = \left[C_{P_0}^{P}\right]^{T} \vec{r}_{cm\to hp}^{\,P} \tag{8}$$

where $\vec{r}_{cm\to hp}^{\,P} = \begin{bmatrix} x_{cm\to hp}^{P} \\ y_{cm\to hp}^{P} \\ z_{cm\to hp}^{P} \end{bmatrix}$ is the vector from the center of mass to the hinge point in probe coordinates. Combining Eqs. (1) and (8) yields

$$x_{cm\to hp}^{P_0} = x_{cm\to hp}^{P}\cos\beta + z_{cm\to hp}^{P}\sin\beta \tag{9a}$$

$$\begin{aligned}y_{cm\to hp}^{P_0} &= x_{cm\to hp}^{P}\sin\beta\sin\alpha + y_{cm\to hp}^{P}\cos\alpha \\ &\quad - z_{cm\to hp}^{P}\cos\beta\sin\alpha\end{aligned} \tag{9b}$$

$$z_{cm\to hp}^{P_0} = -x_{cm\to hp}^{P} \sin\beta\cos\alpha + y_{cm\to hp}^{P} \sin\alpha + z_{cm\to hp}^{P} \cos\beta\cos\alpha \quad (9c)$$

The radial boom mass will be at the same Z location as the hinge point, and in the direction of the X and Y components of the line from the center of mass to the hinge point. Therefore, the vector from the hinge point to the radial boom point mass, $\vec{r}_{hp\to mr}^{P_0}$, in nominal probe frame coordinates can be written as

$$\vec{r}_{hp\to mr}^{P_0} = \frac{L_r}{r_{cm\to hp,XY}^{P_0}} \begin{bmatrix} x_{cm\to hp}^{P_0} \\ y_{cm\to hp}^{P_0} \\ 0 \end{bmatrix} \quad (10)$$

where L_r is the radial boom length and

$$r_{cm\to hp,XY}^{P_0} = \sqrt{\left(x_{cm\to hp}^{P_0}\right)^2 + \left(y_{cm\to hp}^{P_0}\right)^2} \quad (11)$$

Is the radial distance from the central body Z-axis to the appendage hinge point. Eqs. (9) and (10) combine to form the vector from the center of mass to the radial boom tip mass

$$\vec{r}_{cm\to mr}^{P_0} = \vec{r}_{cm\to hp}^{P_0} + \vec{r}_{hp\to mr}^{P_0} = \begin{bmatrix} x_{cm\to hp}^{P_0}\left(1 + \frac{L_r}{r_{cm\to hp,XY}^{P_0}}\right) \\ y_{cm\to hp}^{P_0}\left(1 + \frac{L_r}{r_{cm\to hp,XY}^{P_0}}\right) \\ z_{cm\to hp}^{P_0} \end{bmatrix} \quad (12)$$

Substituting Eq. (11) into Eq. (12) and taking the sum of the squares of the X and Y components yields the squared distance from the spin axis to the tip mass

$$\left|\vec{r}_{cm\to m_r,XY}^{P_0}\right|^2 = \left(x_{cm\to hp}^{P_0}\right)^2 + \left(y_{cm\to hp}^{P_0}\right)^2 + L_r^2 + 2L_r r_{cm\to hp,XY}^{P_0} \quad (13)$$

Using this result, the radial boom contribution to the z-axis inertia for the radial boom tip mass, m_r, can be written as

$$I_{zz0,r} = m_r\left[\left(x_{cm\to hp}^{P_0}\right)^2 + \left(y_{cm\to hp}^{P_0}\right)^2 + L_r^2 + 2L_r r_{cm\to hp,XY}^{P_0}\right] \quad (14)$$

An example of radial boom spin axis inertia as a function of α and β is depicted in Figure 4. Radial booms stabilize spin about the Z-axis.

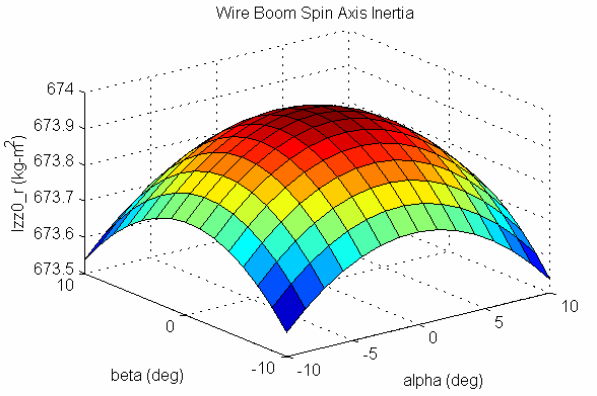

Figure 4: Radial Boom Spin Axis Inertia Example

Taking first partial derivatives of Eq. (14) yields

$$\frac{\partial I_{zz0,r}}{\partial\alpha} = 2m_r\left(x_{cm\to hp}^{P_0}\frac{\partial x_{cm\to hp}^{P_0}}{\partial\alpha} + y_{cm\to hp}^{P_0}\frac{\partial y_{cm\to hp}^{P_0}}{\partial\alpha} + L_r\frac{\partial r_{cm\to hp,XY}^{P_0}}{\partial\alpha}\right) \quad (15a)$$

$$\frac{\partial I_{zz0,r}}{\partial\beta} = 2m_r\left(x_{cm\to hp}^{P_0}\frac{\partial x_{cm\to hp}^{P_0}}{\partial\beta} + y_{cm\to hp}^{P_0}\frac{\partial y_{cm\to hp}^{P_0}}{\partial\beta} + L_r\frac{\partial r_{cm\to hp,XY}^{P_0}}{\partial\beta}\right) \quad (15b)$$

where

$$\frac{\partial x_{cm\to hp}^{P_0}}{\partial\alpha} = 0 \quad (16a)$$

$$\frac{\partial x_{cm\to hp}^{P_0}}{\partial\beta} = -x_{cm\to hp}^{P} \sin\beta + z_{cm\to hp}^{P} \cos\beta \quad (16b)$$

$$\frac{\partial y_{cm\to hp}^{P_0}}{\partial\alpha} = x_{cm\to hp}^{P} \sin\beta\cos\alpha - y_{cm\to hp}^{P} \sin\alpha - z_{cm\to hp}^{P} \cos\beta\cos\alpha \quad (17a)$$

$$\frac{\partial y_{cm\to hp}^{P_0}}{\partial\beta} = x_{cm\to hp}^{P} \cos\beta\sin\alpha + z_{cm\to hp}^{P} \sin\beta\sin\alpha \quad (17b)$$

$$\frac{\partial r_{cm\to hp,XY}^{P_0}}{\partial\alpha}=\frac{1}{r_{cm\to hp,XY}^{P_0}}\left(x_{cm\to hp}^{P_0}\frac{\partial x_{cm\to hp}^{P_0}}{\partial\alpha}+y_{cm\to hp}^{P_0}\frac{\partial y_{cm\to hp}^{P_0}}{\partial\alpha}\right) \quad (18a)$$

$$\frac{\partial r_{cm\to hp,XY}^{P_0}}{\partial\beta}=\frac{1}{r_{cm\to hp,XY}^{P_0}}\left(x_{cm\to hp}^{P_0}\frac{\partial x_{cm\to hp}^{P_0}}{\partial\beta}+y_{cm\to hp}^{P_0}\frac{\partial y_{cm\to hp}^{P_0}}{\partial\beta}\right) \quad (18b)$$

Substituting Eqs. (16) through (18) into Eq. (15) and letting $\alpha=0$ and $\beta=0$ yields

$$\left.\frac{\partial I_{zz0,r}}{\partial\alpha}\right|_{\alpha=0,\beta=0}=2m_r\left(-y_{cm\to hp}^{P}z_{cm\to hp}^{P}-\frac{L_r y_{cm\to hp}^{P}z_{cm\to hp}^{P}}{\sqrt{\left(x_{cm\to hp}^{P}\right)^2+\left(y_{cm\to hp}^{P}\right)^2}}\right) \quad (19a)$$

$$\left.\frac{\partial I_{zz0,r}}{\partial\beta}\right|_{\alpha=0,\beta=0}=2m_r\left(x_{cm\to hp}^{P}z_{cm\to hp}^{P}+\frac{L_r x_{cm\to hp}^{P}z_{cm\to hp}^{P}}{\sqrt{\left(x_{cm\to hp}^{P}\right)^2+\left(y_{cm\to hp}^{P}\right)^2}}\right) \quad (19b)$$

Taking second partial derivatives of Eq. (14) yields

$$\frac{\partial^2 I_{zz0,r}}{\partial\alpha^2}=2m_r\left(\begin{array}{l}\left(\frac{\partial x_{cm\to hp}^{P_0}}{\partial\alpha}\right)^2+x_{cm\to hp}^{P_0}\frac{\partial^2 x_{cm\to hp}^{P_0}}{\partial\alpha^2}\\+\left(\frac{\partial y_{cm\to hp}^{P_0}}{\partial\alpha}\right)^2+y_{cm\to hp}^{P_0}\frac{\partial^2 y_{cm\to hp}^{P_0}}{\partial\alpha^2}\\+L_r\frac{\partial^2 r_{cm\to hp,XY}^{P_0}}{\partial\alpha^2}\end{array}\right) \quad (20a)$$

$$\frac{\partial^2 I_{zz0,r}}{\partial\beta^2}=2m_r\left(\begin{array}{l}\left(\frac{\partial x_{cm\to hp}^{P_0}}{\partial\beta}\right)^2+x_{cm\to hp}^{P_0}\frac{\partial^2 x_{cm\to hp}^{P_0}}{\partial\beta^2}\\+\left(\frac{\partial y_{cm\to hp}^{P_0}}{\partial\beta}\right)^2+y_{cm\to hp}^{P_0}\frac{\partial^2 y_{cm\to hp}^{P_0}}{\partial\beta^2}\\+L_r\frac{\partial^2 r_{cm\to hp,XY}^{P_0}}{\partial\beta^2}\end{array}\right) \quad (20b)$$

where

$$\frac{\partial^2 x_{cm\to hp}^{P_0}}{\partial\alpha^2}=0 \quad (21a)$$

$$\frac{\partial^2 x_{cm\to hp}^{P_0}}{\partial\beta^2}=-x_{cm\to hp}^{P}\cos\beta-z_{cm\to hp}^{P}\sin\beta \quad (21b)$$

$$\frac{\partial^2 y_{cm\to hp}^{P_0}}{\partial\alpha^2}=-x_{cm\to hp}^{P}\sin\beta\sin\alpha-y_{cm\to hp}^{P}\cos\alpha+z_{cm\to hp}^{P}\cos\beta\sin\alpha \quad (22a)$$

$$\frac{\partial^2 y_{cm\to hp}^{P_0}}{\partial\beta^2}=-x_{cm\to hp}^{P}\sin\beta\sin\alpha+z_{cm\to hp}^{P}\cos\beta\sin\alpha \quad (22b)$$

$$\frac{\partial^2 r_{cm\to hp,XY}^{P_0}}{\partial\alpha^2}=\left(\frac{-1}{\left(r_{cm\to hp,XY}^{P_0}\right)^3}\right)\left(x_{cm\to hp}^{P_0}\frac{\partial x_{cm\to hp}^{P_0}}{\partial\alpha}+y_{cm\to hp}^{P_0}\frac{\partial y_{cm\to hp}^{P_0}}{\partial\alpha}\right)^2+\left(\frac{1}{r_{cm\to hp,XY}^{P_0}}\right)\left(\begin{array}{l}\left(\frac{\partial x_{cm\to hp}^{P_0}}{\partial\alpha}\right)^2+x_{cm\to hp}^{P_0}\frac{\partial^2 x_{cm\to hp}^{P_0}}{\partial\alpha^2}\\+\left(\frac{\partial y_{cm\to hp}^{P_0}}{\partial\alpha}\right)^2+y_{cm\to hp}^{P_0}\frac{\partial^2 y_{cm\to hp}^{P_0}}{\partial\alpha^2}\end{array}\right) \quad (23a)$$

$$\frac{\partial^2 r_{cm\to hp,XY}^{P_0}}{\partial\beta^2}=\left(\frac{-1}{\left(r_{cm\to hp,XY}^{P_0}\right)^3}\right)\left(\bar{r}_{cm\to hp,X}^{P_0}\frac{\partial\bar{r}_{cm\to hp,X}^{P_0}}{\partial\beta}+\bar{r}_{cm\to hp,Y}^{P_0}\frac{\partial\bar{r}_{cm\to hp,Y}^{P_0}}{\partial\beta}\right)^2+\left(\frac{1}{r_{cm\to hp,XY}^{P_0}}\right)\left(\begin{array}{l}\left(\frac{\partial x_{cm\to hp}^{P_0}}{\partial\beta}\right)^2+x_{cm\to hp}^{P_0}\frac{\partial^2 x_{cm\to hp}^{P_0}}{\partial\beta^2}\\+\left(\frac{\partial y_{cm\to hp}^{P_0}}{\partial\beta}\right)^2+y_{cm\to hp}^{P_0}\frac{\partial^2 y_{cm\to hp}^{P_0}}{\partial\beta^2}\end{array}\right) \quad (23b)$$

Substituting Eqs. (16), (17), and (21) through (23) into Eq. (20) and letting $\alpha=0$ and $\beta=0$ yields

$$\left.\frac{\partial^2 I_{zz0,r}}{\partial\alpha^2}\right|_{\alpha=0,\beta=0}=2m_r\left(\begin{array}{l}\left(1+\frac{L_r}{\sqrt{\left(x_{cm\to hp}^{P}\right)^2+\left(y_{cm\to hp}^{P}\right)^2}}\right)\\\cdot\left[\left(z_{cm\to hp}^{P}\right)^2-\left(y_{cm\to hp}^{P}\right)^2\right]\\-L_r\frac{\left(y_{cm\to hp}^{P}z_{cm\to hp}^{P}\right)^2}{\left(\sqrt{\left(x_{cm\to hp}^{P}\right)^2+\left(y_{cm\to hp}^{P}\right)^2}\right)^3}\end{array}\right) \quad (24a)$$

$$\left.\frac{\partial^2 I_{zz0,r}}{\partial\beta^2}\right|_{\alpha=0,\beta=0}=2m_r\left(\begin{array}{l}\left(1+\frac{L_r}{\sqrt{\left(x_{cm\to hp}^{P}\right)^2+\left(y_{cm\to hp}^{P}\right)^2}}\right)\\\cdot\left[\left(z_{cm\to hp}^{P}\right)^2-\left(x_{cm\to hp}^{P}\right)^2\right]\\-L_r\frac{\left(x_{cm\to hp}^{P}z_{cm\to hp}^{P}\right)^2}{\left(\sqrt{\left(x_{cm\to hp}^{P}\right)^2+\left(y_{cm\to hp}^{P}\right)^2}\right)^3}\end{array}\right) \quad (24b)$$

Radial boom results were combined with central body and axial boom results in a later section.

Axial Booms

The axial booms were modeled as point masses connected to the central body by flexible massless rods. The vector from the probe center of mass to the undeformed axial boom mass, m_a, on the perturbed central body expressed in nominal probe frame (P_0) coordinates is

$$\vec{r}_{cm\to ma}^{\,P_0} = \begin{bmatrix} x_{cm\to ma}^{P_0} \\ y_{cm\to ma}^{P_0} \\ z_{cm\to ma}^{P_0} \end{bmatrix} = \left[C_{P_0}^{P}\right]^T \vec{r}_{cm\to ma}^{\,P} \qquad (25)$$

where $\vec{r}_{cm\to ma}^{\,P} = \begin{bmatrix} x_{cm\to ma}^{P} \\ y_{cm\to ma}^{P} \\ z_{cm\to ma}^{P} \end{bmatrix}$ is the vector from the center of mass to the axial boom mass in probe coordinates. Combining Eqs. (1) and (25) yields

$$x_{cm\to ma}^{P_0} = x_{cm\to ma}^{P}\cos\beta + z_{cm\to ma}^{P}\sin\beta \qquad (26a)$$

$$y_{cm\to ma}^{P_0} = x_{cm\to ma}^{P}\sin\beta\sin\alpha + y_{cm\to ma}^{P}\cos\alpha - z_{cm\to ma}^{P}\cos\beta\sin\alpha \qquad (26b)$$

$$z_{cm\to ma}^{P_0} = -x_{cm\to ma}^{P}\sin\beta\cos\alpha + y_{cm\to ma}^{P}\sin\alpha + z_{cm\to ma}^{P}\cos\beta\cos\alpha \qquad (26c)$$

Centrifugal force on the axial boom mass will be countered by the force due to bending of the boom. Therefore

$$m_a\omega_{spin}^2\left|\vec{r}_{cm\to ma,XY}^{\,P_0}\right|_d \cong k_x\left(\left|\vec{r}_{cm\to ma,XY}^{\,P_0}\right|_d - \left|\vec{r}_{cm\to ma,XY}^{\,P_0}\right|_u\right) \qquad (27)$$

Where ω_{spin} is the probe spin rate, k_x is the axial boom stiffness, and $\left|\vec{r}_{cm\to ma,XY}^{\,P_0}\right|_u$ is the radius of the "orbit" of the undeformed axial boom mass

$$\left|\vec{r}_{cm\to ma,XY}^{\,P_0}\right|_u = \sqrt{\left(x_{cm\to ma}^{P_0}\right)^2 + \left(y_{cm\to ma}^{P_0}\right)^2} \qquad (28)$$

and $\left|\vec{r}_{cm\to ma,XY}^{\,P_0}\right|_d$ is the radius of the "orbit" of the deformed axial boom mass. Solving Eq. (27) for this deformed axial boom mass radius yields

$$\left|\vec{r}_{cm\to ma,XY}^{\,P_0}\right|_d = \left(\frac{k_x}{k_x - m_a\omega_{spin}^2}\right)\left|\vec{r}_{cm\to ma,XY}^{\,P_0}\right|_u \qquad (29)$$

Letting $k_x = m_a\Omega_n^2$ for cantilevered boom resonance† in Eq. (29) yields

$$\left|\vec{r}_{cm\to ma,XY}^{\,P_0}\right|_d = \frac{1}{\left(1 - \omega_{spin}^2/\Omega_n^2\right)}\left|\vec{r}_{cm\to ma,XY}^{\,P_0}\right|_u \qquad (30)$$

Using this result, the axial boom contribution to the Z-axis inertia can be written as

$$I_{zz0,a} = m_a\left|\vec{r}_{cm\to ma,XY}^{\,P_0}\right|_d^2 = \frac{m_a}{\left(1 - \omega_{spin}^2/\Omega_n^2\right)^2}\left|\vec{r}_{cm\to ma,XY}^{\,P_0}\right|_u^2 \qquad (31)$$

An example of the axial boom spin axis inertia as a function of α and β is depicted in Figure 5. Axial booms have a destabilizing influence on spin about the Z-axis.

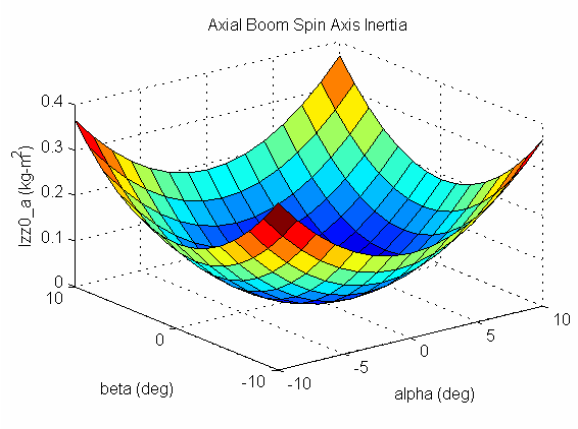

Figure 5: Axial Boom Spin Axis Inertia Example

Taking first partial derivatives of Eq. (31) yields

$$\frac{\partial I_{zz0,a}}{\partial\alpha} = \frac{2m_a}{\left(1 - \omega_{spin}^2/\Omega_n^2\right)^2}\left|\vec{r}_{cm\to ma,XY}^{\,P_0}\right|_u \frac{\partial\left|\vec{r}_{cm\to ma,XY}^{\,P_0}\right|_u}{\partial\alpha} \qquad (32a)$$

$$\frac{\partial I_{zz0,a}}{\partial\beta} = \frac{2m_a}{\left(1 - \omega_{spin}^2/\Omega_n^2\right)^2}\left|\vec{r}_{cm\to ma,XY}^{\,P_0}\right|_u \frac{\partial\left|\vec{r}_{cm\to ma,XY}^{\,P_0}\right|_u}{\partial\beta} \qquad (32b)$$

where

$$\frac{\partial x_{cm\to ma}^{P_0}}{\partial\alpha} = 0 \qquad (33a)$$

† Dr. David Pankow, University California at Berkeley

$$\frac{\partial x_{cm\to ma}^{P_0}}{\partial \beta} = -x_{cm\to ma}^{P} \sin\beta + z_{cm\to ma}^{P} \cos\beta \tag{33b}$$

$$\frac{\partial y_{cm\to ma}^{P_0}}{\partial \alpha} = x_{cm\to ma}^{P} \sin\beta\cos\alpha - y_{cm\to ma}^{P} \sin\alpha - z_{cm\to ma}^{P} \cos\beta\cos\alpha \tag{34a}$$

$$\frac{\partial y_{cm\to ma}^{P_0}}{\partial \beta} = x_{cm\to ma}^{P} \cos\beta\sin\alpha + z_{cm\to ma}^{P} \sin\beta\sin\alpha \tag{34b}$$

$$\frac{\partial \left|\vec{r}_{cm\to ma,XY}^{\,P_0}\right|_u}{\partial \alpha} = \left(\frac{1}{\left|\vec{r}_{cm\to ma,XY}^{\,P_0}\right|_u}\right)\begin{pmatrix} x_{cm\to ma}^{P_0} \dfrac{\partial x_{cm\to ma}^{P_0}}{\partial \alpha} \\ + y_{cm\to ma}^{P_0} \dfrac{\partial y_{cm\to ma}^{P_0}}{\partial \alpha} \end{pmatrix} \tag{35a}$$

$$\frac{\partial \left|\vec{r}_{cm\to ma,XY}^{\,P_0}\right|_u}{\partial \beta} = \left(\frac{1}{\left|\vec{r}_{cm\to ma,XY}^{\,P_0}\right|_u}\right)\begin{pmatrix} x_{cm\to ma}^{P_0} \dfrac{\partial x_{cm\to ma}^{P_0}}{\partial \beta} \\ + y_{cm\to ma}^{P_0} \dfrac{\partial y_{cm\to ma}^{P_0}}{\partial \beta} \end{pmatrix} \tag{35b}$$

Substituting Eq. (28) and (33) through (35) into Eq. (32) and letting $\alpha = 0$ and $\beta = 0$ yields

$$\left.\frac{\partial I_{zz0,a}}{\partial \alpha}\right|_{\alpha=0,\beta=0} = -\frac{2m_a y_{cm\to ma}^{P} z_{cm\to ma}^{P}}{\left(1 - \omega_{spin}^2 / \Omega_n^2\right)^2} \tag{36a}$$

$$\left.\frac{\partial I_{zz0,a}}{\partial \beta}\right|_{\alpha=0,\beta=0} = \frac{2m_a x_{cm\to ma}^{P} z_{cm\to ma}^{P}}{\left(1 - \omega_{spin}^2 / \Omega_n^2\right)^2} \tag{36b}$$

Taking second partial derivatives of Eq. (31) yields

$$\frac{\partial^2 I_{zz0,a}}{\partial \alpha^2} = \frac{2m_a}{\left(1 - \omega_{spin}^2 / \Omega_n^2\right)^2} \cdot \left[\left(\frac{\partial \left|\vec{r}_{cm\to ma,XY}^{\,P_0}\right|_u}{\partial \alpha}\right)^2 + \left|\vec{r}_{cm\to ma,XY}^{\,P_0}\right|_u \frac{\partial^2 \left|\vec{r}_{cm\to ma,XY}^{\,P_0}\right|_u}{\partial \alpha^2}\right] \tag{37a}$$

$$\frac{\partial^2 I_{zz0,a}}{\partial \beta^2} = \frac{2m_a}{\left(1 - \omega_{spin}^2 / \Omega_n^2\right)^2} \cdot \left[\left(\frac{\partial \left|\vec{r}_{cm\to ma,XY}^{\,P_0}\right|_u}{\partial \beta}\right)^2 + \left|\vec{r}_{cm\to ma,XY}^{\,P_0}\right|_u \frac{\partial^2 \left|\vec{r}_{cm\to ma,XY}^{\,P_0}\right|_u}{\partial \beta^2}\right] \tag{37b}$$

where

$$\frac{\partial^2 x_{cm\to ma}^{P_0}}{\partial \alpha^2} = 0 \tag{38a}$$

$$\frac{\partial^2 x_{cm\to ma}^{P_0}}{\partial \beta^2} = -x_{cm\to ma}^{P} \cos\beta - z_{cm\to ma}^{P} \sin\beta \tag{38b}$$

$$\frac{\partial^2 y_{cm\to ma}^{P_0}}{\partial \alpha^2} = -x_{cm\to ma}^{P} \sin\beta\sin\alpha - y_{cm\to ma}^{P} \cos\alpha + z_{cm\to ma}^{P} \cos\beta\sin\alpha \tag{39a}$$

$$\frac{\partial^2 y_{cm\to ma}^{P_0}}{\partial \beta^2} = -x_{cm\to ma}^{P} \sin\beta\sin\alpha + z_{cm\to ma}^{P} \cos\beta\sin\alpha \tag{39b}$$

$$\frac{\partial^2 \left|\vec{r}_{cm\to ma,XY}^{\,P_0}\right|_u}{\partial \alpha^2} = \left[\frac{-1}{\left|\vec{r}_{cm\to ma,XY}^{\,P_0}\right|_u^3}\right]\left(x_{cm\to ma}^{P_0} \frac{\partial x_{cm\to ma}^{P_0}}{\partial \alpha} + y_{cm\to ma}^{P_0} \frac{\partial y_{cm\to ma}^{P_0}}{\partial \alpha}\right)^2 + \left(\frac{1}{\left|\vec{r}_{cm\to ma,XY}^{\,P_0}\right|_u}\right)\begin{bmatrix} \left(\dfrac{\partial x_{cm\to ma}^{P_0}}{\partial \alpha}\right)^2 + x_{cm\to ma}^{P_0} \dfrac{\partial^2 x_{cm\to ma}^{P_0}}{\partial \alpha^2} \\ + \left(\dfrac{\partial y_{cm\to ma}^{P_0}}{\partial \alpha}\right)^2 + y_{cm\to ma}^{P_0} \dfrac{\partial^2 y_{cm\to ma}^{P_0}}{\partial \alpha^2} \end{bmatrix} \tag{40a}$$

$$\frac{\partial^2 \left|\vec{r}_{cm\to ma,XY}^{\,P_0}\right|_u}{\partial \beta^2} = \left[\frac{-1}{\left|\vec{r}_{cm\to ma,XY}^{\,P_0}\right|_u^3}\right]\left(x_{cm\to ma}^{P_0} \frac{\partial x_{cm\to ma}^{P_0}}{\partial \beta} + y_{cm\to ma}^{P_0} \frac{\partial y_{cm\to ma}^{P_0}}{\partial \beta}\right)^2 + \left(\frac{1}{\left|\vec{r}_{cm\to ma,XY}^{\,P_0}\right|_u}\right)\begin{bmatrix} \left(\dfrac{\partial x_{cm\to ma}^{P_0}}{\partial \beta}\right)^2 + x_{cm\to ma}^{P_0} \dfrac{\partial^2 x_{cm\to ma}^{P_0}}{\partial \beta^2} \\ + \left(\dfrac{\partial y_{cm\to ma}^{P_0}}{\partial \beta}\right)^2 + y_{cm\to ma}^{P_0} \dfrac{\partial^2 y_{cm\to ma}^{P_0}}{\partial \beta^2} \end{bmatrix} \tag{40b}$$

Substituting Eqs. (28), (35), and (38) through (40) into Eq. (37) and letting $\alpha = 0$ and $\beta = 0$ yields

$$\left.\frac{\partial^2 I_{zz0,a}}{\partial \alpha^2}\right|_{\alpha=0,\beta=0} = \frac{2m_a}{\left(1 - \omega_{spin}^2 / \Omega_n^2\right)^2}\left[\left(z_{cm\to ma}^{P}\right)^2 - \left(y_{cm\to ma}^{P}\right)^2\right] \tag{41a}$$

$$\left.\frac{\partial^2 I_{zz0,a}}{\partial \beta^2}\right|_{\alpha=0,\beta=0} = \frac{2m_a}{\left(1 - \omega_{spin}^2 / \Omega_n^2\right)^2}\left[\left(z_{cm\to ma}^{P}\right)^2 - \left(x_{cm\to ma}^{P}\right)^2\right] \tag{41b}$$

Axial boom results were combined with central body and radial boom results in the following section.

Aggregate System

The total spin-axis moment of inertia is the sum of the central body, radial boom, and axial boom inertia contributions from Eqs. (3), (14), and (31) (with indexing for radial and axial booms)

$$\begin{aligned} I_{zz0} &= I_{xx}^{P}\sin^2\beta\cos^2\alpha + I_{yy}^{P}\sin^2\alpha + I_{zz}^{P}\cos^2\beta\cos^2\alpha \\ &\quad - I_{xy}^{P}\sin\beta\sin 2\alpha - I_{xz}^{P}\sin 2\beta\cos^2\alpha + I_{yz}^{P}\cos\beta\sin 2\alpha \\ &\quad + \sum_{i=1}^{n_r} m_{r,i}\left[\left(x_{cm\to hp,i}^{P_0}\right)^2 + \left(y_{cm\to hp,i}^{P_0}\right)^2 + L_{r,i}^2 + 2L_{r,i}r_{cm\to hp,XY,i}^{P_0}\right] \\ &\quad + \sum_{i=1}^{n_a}\frac{m_{a,i}}{\left(1-\omega_{spin}^2/\Omega_{n,i}^2\right)^2}\left[\begin{array}{l}\left(x_{cm\to ma,i}^{P}\right)^2 + \left(y_{cm\to ma,i}^{P}\right)^2\cos^2\alpha \\ +\left(z_{cm\to ma,i}^{P}\right)^2\left(\sin^2\beta + \cos^2\beta\sin^2\alpha\right) \\ + x_{cm\to ma,i}^{P}y_{cm\to ma,i}^{P}\sin\beta\sin 2\alpha \\ - y_{cm\to ma,i}^{P}z_{cm\to ma,i}^{P}\cos\beta\sin 2\alpha \\ + x_{cm\to ma,i}^{P}z_{cm\to ma,i}^{P}\sin 2\beta\cos^2\alpha\end{array}\right] \end{aligned} \tag{42}$$

where n_r is the number of radial booms and n_a is the number of axial booms.

An example of the total spin axis inertia as a function of α and β is depicted in Figure 6. The destabilizing effect of axial booms is sufficiently offset by the stabilizing influence of the radial booms and central body in this example.

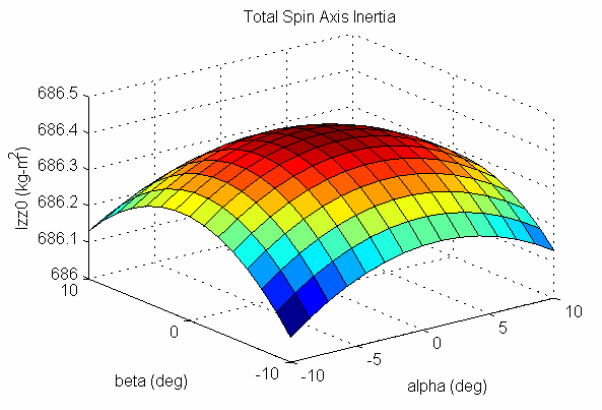

Figure 6: Total Spin Axis Inertia Example

The total first partial derivatives of the Z-axis inertia for $\alpha = 0$ and $\beta = 0$ were obtained by combining Eqs. (5), (19), and (36) (with indexing for radial and axial booms)

$$\left.\frac{\partial I_{zz0}}{\partial\alpha}\right|_{\alpha=0,\beta=0} = 2I_{yz}^{P} - \sum_{i=1}^{n_r}2F_{r,i}m_{r,i}y_{cm\to hp,i}^{P}z_{cm\to hp,i}^{P} - \sum_{i=1}^{n_a}2F_{a,i}^2m_{a,i}y_{cm\to ma,i}^{P}z_{cm\to ma,i}^{P} \tag{43a}$$

$$\frac{\partial I_{zz0}}{\partial\beta} = -2I_{xz}^{P} + \sum_{i=1}^{n_r}2F_{r,i}m_{r,i}x_{cm\to hp,i}^{P}z_{cm\to hp,i}^{P} + \sum_{i=1}^{n_a}2F_{a,i}^2m_{a,i}x_{cm\to ma,i}^{P}z_{cm\to ma,i}^{P} \tag{43b}$$

where

$$F_{r,i} = \left(\frac{\sqrt{\left(x_{cm\to hp,i}^{P}\right)^2 + \left(y_{cm\to hp,i}^{P}\right)^2} + L_{r,i}}{\sqrt{\left(x_{cm\to hp,i}^{P}\right)^2 + \left(y_{cm\to hp,i}^{P}\right)^2}}\right) \tag{44}$$

$$F_{a,i}^2 = \frac{1}{\left(1-\omega_{spin}^2/\Omega_{n,i}^2\right)^2} \tag{45}$$

Stable spin about the central body Z-axis requires Eq. (43) to equal zero.

$$I_{yz}^{P} - \sum_{i=1}^{n_r}F_{r,i}m_{r,i}y_{cm\to hp,i}^{P}z_{cm\to hp,i}^{P} - \sum_{i=1}^{n_a}F_{a,i}^2m_{a,i}y_{cm\to ma,i}^{P}z_{cm\to ma,i}^{P} = 0 \tag{46a}$$

$$-I_{xz}^{P} + \sum_{i=1}^{n_r}F_{r,i}m_{r,i}x_{cm\to hp,i}^{P}z_{cm\to hp,i}^{P} + \sum_{i=1}^{n_a}F_{a,i}^2m_{a,i}x_{cm\to ma,i}^{P}z_{cm\to ma,i}^{P} = 0 \tag{46b}$$

The first derivative stability criteria in Eq. (46) are necessary but not sufficient for spin about the Z-axis. Since they were derived by setting α and β to zero, $\alpha \neq 0$ and $\beta \neq 0$ if these equalities are not satisfied. There will be a steady state principal axis offset from the probe Z-axis if these equalities are not satisfied.

The total second partial derivatives of the Z-axis inertia for $\alpha = 0$ and $\beta = 0$ were obtained by combining Eqs. (7), (24), and (41) (with indexing for radial and axial booms)

$$\left.\frac{\partial^2 I_{zz0}}{\partial \alpha^2}\right|_{\alpha=0,\beta=0} = 2\left(I_{yy}^P - I_{zz}^P\right) + \sum_{i=1}^{n_r} 2m_{r,i}\begin{pmatrix} F_{r,i}\left[\left(z_{cm\to hp,i}^P\right)^2 - \left(y_{cm\to hp,i}^P\right)^2\right] \\ -L_{r,i}\dfrac{\left(y_{cm\to hp,i}^P z_{cm\to hp,i}^P\right)^2}{\left(\sqrt{\left(x_{cm\to hp,i}^P\right)^2 + \left(y_{cm\to hp,i}^P\right)^2}\right)^3} \end{pmatrix} + \sum_{i=1}^{n_a} 2m_{a,i}F_{a,i}^2\left[\left(z_{cm\to ma,i}^P\right)^2 - \left(y_{cm\to ma,i}^P\right)^2\right] \quad (47a)$$

$$\left.\frac{\partial^2 I_{zz0}}{\partial \beta^2}\right|_{\alpha=0,\beta=0} = 2\left(I_{xx}^P - I_{zz}^P\right) + \sum_{i=1}^{n_r} 2m_{r,i}\begin{pmatrix} F_{r,i}\left[\left(z_{cm\to hp,i}^P\right)^2 - \left(x_{cm\to hp,i}^P\right)^2\right] \\ -L_{r,i}\dfrac{\left(x_{cm\to hp,i}^P z_{cm\to hp,i}^P\right)^2}{\left(\sqrt{\left(x_{cm\to hp,i}^P\right)^2 + \left(y_{cm\to hp,i}^P\right)^2}\right)^3} \end{pmatrix} + \sum_{i=1}^{n_a} 2m_{a,i}F_{a,i}^2\left[\left(z_{cm\to ma,i}^P\right)^2 - \left(x_{cm\to ma,i}^P\right)^2\right] \quad (47b)$$

Stable spin about the central body Z-axis requires Eq. 47 to be negative.

$$I_{yy}^P - I_{zz}^P + \sum_{i=1}^{n_r} m_{r,i}\begin{pmatrix} F_{r,i}\left[\left(z_{cm\to hp,i}^P\right)^2 - \left(y_{cm\to hp,i}^P\right)^2\right] \\ -L_{r,i}\dfrac{\left(y_{cm\to hp,i}^P z_{cm\to hp,i}^P\right)^2}{\left(\sqrt{\left(x_{cm\to hp,i}^P\right)^2 + \left(y_{cm\to hp,i}^P\right)^2}\right)^3} \end{pmatrix} + \sum_{i=1}^{n_a} m_{a,i}F_{a,i}^2\left[\left(z_{cm\to ma,i}^P\right)^2 - \left(y_{cm\to ma,i}^P\right)^2\right] < 0 \quad (48a)$$

$$I_{xx}^P - I_{zz}^P + \sum_{i=1}^{n_r} m_{r,i}\begin{pmatrix} F_{r,i}\left[\left(z_{cm\to hp,i}^P\right)^2 - \left(x_{cm\to hp,i}^P\right)^2\right] \\ -L_{r,i}\dfrac{\left(x_{cm\to hp,i}^P z_{cm\to hp,i}^P\right)^2}{\left(\sqrt{\left(x_{cm\to hp,i}^P\right)^2 + \left(y_{cm\to hp,i}^P\right)^2}\right)^3} \end{pmatrix} + \sum_{i=1}^{n_a} m_{a,i}F_{a,i}^2\left[\left(z_{cm\to ma,i}^P\right)^2 - \left(x_{cm\to ma,i}^P\right)^2\right] < 0 \quad (48b)$$

Effective Inertias

Stability criteria can be expressed as a function of axial and transverse effective inertias, C_{eff} and A_{eff}, respectively, as follows

$$\frac{C_{eff,\alpha}}{A_{eff,\alpha}} > 1 \quad (49a)$$

$$\frac{C_{eff,\beta}}{A_{eff,\beta}} > 1 \quad (49b)$$

where the subscripts α and β indicate the second partial derivative from which the respective effective inertia was derived. To derive effective inertias from second partial derivatives of the spin axis moment of inertia, radial boom contributions due to vertical offset from the center of mass were treated as contributions to the transverse inertia and axial boom contributions due to lateral offset were treated as contributions to the spin axis inertia. Terms that fit both categories were combined with the effective inertia they would increase. Categorizing terms of Eq. (48) in this manner yields

$$A_{eff,\alpha} = I_{yy}^P + \sum_{i=1}^{n_r} F_{r,i}m_{r,i}\left(z_{cm\to hp,i}^P\right)^2 + \sum_{i=1}^{n_a} F_{a,i}^2 m_{a,i}\left(z_{cm\to ma,i}^P\right)^2 \quad (50a)$$

$$C_{eff,\alpha} = I_{zz}^P + \sum_{i=1}^{n_r} m_{r,i}\begin{pmatrix} F_{r_i}\left(y_{cm\to hp,i}^P\right)^2 \\ +L_{r,i}\dfrac{\left(y_{cm\to hp,i}^P z_{cm\to hp,i}^P\right)^2}{\left(\sqrt{\left(x_{cm\to hp,i}^P\right)^2 + \left(y_{cm\to hp,i}^P\right)^2}\right)^3} \end{pmatrix} + \sum_{i=1}^{n_a} F_{a,i}^2 m_{a,i}\left(y_{cm\to ma,i}^P\right)^2 \quad (50b)$$

$$A_{eff,\beta} = I_{xx}^P + \sum_{i=1}^{n_r} F_{r,i}m_{r,i}\left(z_{cm\to hp,i}^P\right)^2 + \sum_{i=1}^{n_a} F_{a,i}^2 m_{a,i}\left(z_{cm\to ma,i}^P\right)^2 \quad (50c)$$

$$C_{eff,\beta} = I_{zz}^P + \sum_{i=1}^{n_r} m_{r,i}\begin{pmatrix} F_{r,i}\left(x_{cm\to hp,i}^P\right)^2 \\ +L_{r,i}\dfrac{\left(x_{cm\to hp,i}^P z_{cm\to hp,i}^P\right)^2}{\left(\sqrt{\left(x_{cm\to hp,i}^P\right)^2 + \left(y_{cm\to hp,i}^P\right)^2}\right)^3} \end{pmatrix} + \sum_{i=1}^{n_a} F_{a,i}^2 m_{a,i}\left(x_{cm\to ma,i}^P\right)^2 \quad (50d)$$

The stability margin can be computed based on the ratios of effective inertias per Eqs. (49) and (50). These second derivative criteria ensure the surface of spin axis inertia as a function of α and β is concave down in the vicinity of $\alpha = 0$ and $\beta = 0$. Therefore, even if there is a small steady state principal axis offset (i.e., $\alpha \neq 0$ and/or $\beta \neq 0$), satisfying Eq. (49) ensures spin will be stable even with a small principal axis offset.

Configuration Dependent Simplifications

Several configuration dependent simplifications were presented in this section. For example, for identical radial booms parallel to the probe X and Y axes with a hinge point located a distance a from the Z-axis and all at the same Z location (not the final THEMIS configuration, which has two unequal length pairs)

$$x^P_{cm\to hp,1} = a,\ x^P_{cm\to hp,2} = 0,\ x^P_{cm\to hp,3} = -a,\ x^P_{cm\to hp,4} = 0 \quad (51)$$

$$y^P_{cm\to hp,1} = 0,\ y^P_{cm\to hp,2} = a,\ y^P_{cm\to hp,3} = 0,\ y^P_{cm\to hp,4} = a \quad (52)$$

$$z^P_{cm\to hp,1} = z^P_{cm\to hp,2} = z^P_{cm\to hp,3} = z^P_{cm\to hp,4} = z^P_{cm\to hp} \quad (53)$$

$$m_{r,1} = m_{r,2} = m_{r,3} = m_{r,4} = m_r \quad (54)$$

Assuming the X and Y axis radial boom pairs can be different lengths, then

$$L_{r,1} = L_{r,3} = L_x,\ L_{r,2} = L_{r,4} = L_y \quad (55)$$

Substitution of Eqs. (51) through (53) and (55) into Eqs. (44) and (45) yields

$$F_{r,1} = F_{r,3} = F_x = \left(\frac{a + L_x}{a}\right) \quad (56)$$

$$F_{r,2} = F_{r,4} = F_y = \left(\frac{a + L_y}{a}\right) \quad (57)$$

For undeformed axial booms along the probe Z-axis,

$$x^P_{cm\to ma,1} = x^P_{cm\to ma,2} = 0,\ y^P_{cm\to ma,1} = y^P_{cm\to ma,2} = 0 \quad (58)$$

Substituting Eqs. (51) through (54), (56) and (57) into Eq. (46) yields the following stability criteria

$$I^P_{yz} = 0 \quad (59a)$$

$$I^P_{xz} = 0 \quad (59b)$$

The central body must be perfectly spin balanced for configurations with symmetric booms having stable spin about the central body Z-axis.

Substituting Eqs. (51) through (54), (56) and (57) into Eq. (50) yields

$$A_{eff,\alpha} = I^P_{yy} + 2F_x m_r \left(z^P_{cm\to hp}\right)^2 + 2m_r \left(z^P_{cm\to hp}\right)^2 + \sum_{i=1}^{n_a} m_{a,i} F^2_{a,i} \left(z^P_{cm\to ma,i}\right)^2 \quad (60a)$$

$$C_{eff,\alpha} = I^P_{zz} + 2F_y m_r a^2 \quad (60b)$$

$$A_{eff,\beta} = I^P_{xx} + 2m_r \left(z^P_{cm\to hp}\right)^2 + 2F_y m_r \left(z^P_{cm\to hp}\right)^2 + \sum_{i=1}^{n_a} m_{a,i} F^2_{a,i} \left(z^P_{cm\to ma,i}\right)^2 \quad (60c)$$

$$C_{eff,\beta} = I^P_{zz} + 2F_x m_r a^2 \quad (60d)$$

For radial booms hinged at the axial location of the center of mass (in general, not the case for THEMIS), the following simplifications apply

$$z^P_{cm\to hp,1} = z^P_{cm\to hp,2} = z^P_{cm\to hp,3} = z^P_{cm\to hp,4} = 0 \quad (61)$$

Substituting Eq. (61) into Eq. (60) yields

$$A_{eff,\alpha} = I^P_{yy} + \sum_{i=1}^{n_a} F^2_{a,i} m_{a,i} \left(z^P_{cm\to ma,i}\right)^2 \quad (62a)$$

$$C_{eff,\alpha} = I^P_{zz} + 2F_y m_r a^2 \quad (62b)$$

$$A_{eff,\beta} = I^P_{xx} + \sum_{i=1}^{n_a} F^2_{a,i} m_{a,i} \left(z^P_{cm\to ma,i}\right)^2 \quad (62c)$$

$$C_{eff,\beta} = I^P_{zz} + 2F_x m_r a^2 \quad (62d)$$

For axial booms identical and equidistant from the center of mass (not the case for THEMIS), the following simplifications apply

$$z^P_{cm\to ma,1} = z^P_{cm\to ma,2} = z^P_{cm\to ma} \quad (63)$$

$$F^2_{a,1} = F^2_{a,2} = F^2_a \quad (64)$$

$$m_{a,1} = m_{a,2} = m_a \quad (65)$$

Substituting Eqs. (63) through (65) into Eq. (62) yields

$$A_{eff,\alpha} = I^P_{yy} + 2F^2_a m_a \left(z^P_{cm\to ma}\right)^2 \quad (66a)$$

$$C_{eff,\alpha} = I^P_{zz} + 2F_y m_r a^2 \quad (66b)$$

$$A_{eff,\beta} = I^P_{xx} + 2F^2_a m_a \left(z^P_{cm\to ma}\right)^2 \quad (66c)$$

$$C_{eff,\beta} = I^P_{zz} + 2F_x m_r a^2 \quad (66d)$$

Optimizing Unequal Radial Boom Pairs

Stability criteria in Eq. (48) can be used to determine optimum axes for the long and short radial boom pairs based on central body transverse inertias. The transverse inertia I_{xx}^P is countered by the X-axis boom pair $\left[\sum_{i=1}^{n_r} F_{r,i} m_{r,i} \left(x_{cm\to hp,i}^P\right)^2\right]$ and I_{yy}^P is countered by the Y-axis boom pair $\left[\sum_{i=1}^{n_r} F_{r,i} m_{r,i} \left(y_{cm\to hp,i}^P\right)^2\right]$. Therefore, if I_{xx}^P is larger than I_{yy}^P, the longer booms should be placed parallel to the probe X-axis and shorter booms should be placed on the Y-axis. Conversely, if I_{yy}^P is larger than I_{xx}^P, the longer booms should be placed parallel to the probe Y-axis and the shorter booms should be placed on the X-axis.

BOOM MODELING

Analytical formulas in the previous section assume equivalent massless appendages with tip masses. The following sections provide equations for conversion of booms properties to idealized boom properties.

Radial Boom Tip Mass

The radial booms were modeled as point masses at the center of percussion. That is, the boom length was set to the ratio of the second moment and the first moment

$$L_r = \frac{J_{hp}}{c_{hp}} \tag{67}$$

where J_{hp} is the second mass moment (inertia) of boom about the hinge point and c_{hp} is first moment of boom about the hinge point.

The tip mass was set to match the boom inertia

$$m_r = \frac{J_{hp}}{L_r^2} \tag{68}$$

Axial Boom Tip Mass

The idealized model tip mass, m_a, was set equal to the actual tip mass, $m_{a,tip}$, plus one third of the total boom mass, $m_{a,total}$, remaining ‡

$$m_a = m_{a,tip} + \frac{1}{3}\left(m_{a,total} - m_{a,tip}\right) \tag{69}$$

The boom length was adjusted to match the inertia of the boom about its attachment point $\left(J_{hp}\right)$

$$L_a = \sqrt{\frac{J_{hp}}{m_a}} \tag{70}$$

So the axial offset of the axial boom tip mass from the probe center of mass becomes

$$z_{cm\to ma}^P = z_{cm\to hp}^P \pm \sqrt{\frac{J_{hp}}{m_a}} \tag{71}$$

where $z_{cm\to hp}^P$ is the offset of the axial boom attachment point from the probe center of mass in the Z-direction. The plus and minus symbols apply for axial booms in the positive and negative spacecraft Z-directions, respectively.

Axial Boom Flexibility

The axial boom derivation section had the flexible axial boom modeled with a stiffness $k_x = m_a \Omega_n^2$ [N/m], which yields the restoring torque about the attachment point, $T = k_x r_a L_a$. The simple simulation model has the axial boom modeled as a rigid appendage with a 2-degrees of freedom joint having a stiffness $k_\theta = \frac{3EI}{L_a}$ [N-m], which yields the restoring torque about the attachment point, $T = k_\theta \theta$ (Figure 7). Equating these torques and employing $\theta \cong \sin\theta \cong \frac{r_a}{L_a}$ yields

$$k_\theta = \frac{3EI}{L_a} = L_a^2 k_x = m_a L_a^2 \Omega_n^2 \tag{72}$$

‡ Dr. David Pankow, University California at Berkeley

So the boom resonant frequency can be expressed in terms of mechanical properties as

$$\Omega_n = \frac{1}{L_a}\sqrt{\frac{k_\theta}{m_a}} = \frac{1}{L_a}\sqrt{\frac{3EI}{m_a L_a}} \qquad (73)$$

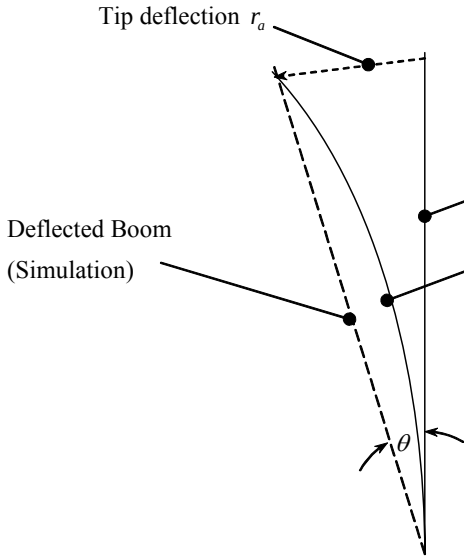

Figure 7: Axial Boom Bending

APPLICATIONS OF STABILITY CRITERIA

THEMIS probes were modeled as central bodies with two magnetometer booms, four radial wire booms (+X, + Y, -X, -Y), two axial stacer booms (+Z, -Z), and two off-axis fuel tanks (2nd and 4th quadrant). Due to the high stiffness of the magnetometer booms and mounts, magnetometer boom properties were included in the rigid central body mass properties. Propellant in off-axis tanks, which could be treated as additional radial booms, provides added stability. Therefore, fuel was not included in the stability analysis because the empty propellant tank configurations are limiting cases.

Analyses were performed for the THEMIS probes in all limiting configurations defined in the mission requirements. Stowed probes and probes with magnetometer booms deployed were analyzed as single rigid bodies. The deployment sequence added many intermediate configurations to the stowed and fully deployed configurations. In addition, off-nominal configurations (e.g., configurations for which one boom failed to deploy) were considered. Sensitivity to variations of radial boom length, axial boom length, and central body inertias was also assessed.

Analyses included calculation of the ratio of spin axis to transverse axis inertia (effective inertia ratio for the coupled multi-body configurations) using analytical formulas and simulation results. Principal axis and center of mass offsets for multi-body configurations were estimated from simulations. Effective inertias from simulations were computed from results of a nutating system using the following equation

$$\frac{C_{eff}}{A_{eff}} = \frac{\omega_{nut}}{\omega_{spin}} + 1 \qquad (74)$$

where ω_{nut} is the nutation frequency determined from the Fast Fourier Transform of the simulated angular velocity for simulations with the spin rate ω_{spin}. Stability was analyzed for spin rates of 2 and 25 RPM.

Coupled multi-body simulations with Swales developed Simulink models, validated using MSC.ADAMS software, were 500 seconds in duration with output at 0.1 second time steps. This resulted in frequency resolution of 0.002 Hz and inertia ratio resolution of 0.060 at 2 RPM and 0.005 at 25 RPM.

Sensitivity Analysis

To further establish "stability margins," the stability analyses were performed with the following variants of the nominal component mass properties:

- Axial boom main stacer length was changed by 0.1 m increments with other parameters nominal. Axial boom mass properties were adjusted accordingly.
- Central body axial inertia (I_{zz}) was changed in 0.5 kg-m^2 decrements with other parameters nominal.
- Central body X-axis transverse inertia (I_{xx}) was changed in 0.5 kg-m^2 increments with other parameters nominal.
- Central body Y-axis transverse inertia (I_{yy}) was changed in 0.5 kg-m^2 increments through nominal, with other parameters nominal.
- Radial boom inner section length was changed in 0.5 m decrements with other parameters nominal. Radial boom mass properties were adjusted accordingly.
- All of the above parameters (i.e., axial boom main stacer length, central body axial and transverse axis inertias, and radial boom inner section length) were varied together in

1 % increments. Parameter changes had +1% increments for axial boom length and transverse axis inertias and -1% increments (i.e., decrements) for axial inertia and radial boom length so each configuration had progressively lower effective inertia ratio.

These variations were applied to the fully deployed configuration and WB +Y failed configurations.

Examples

A small subset of the THEMIS results were presented in this paper to illustrate use of the stability criteria derived herein. In particular, results were given for the following configurations:

- Magnetometer booms deployed, all other booms stowed (single rigid body) (SBN)
- Fully deployed (central body + 4 radial booms + 2 axial booms configuration) (MBN)
- Magnetometer booms deployed, three radial booms fully deployed, one radial boom stowed, and both axial booms deployed (central body + 3 radial booms + 2 axial booms configuration) (MBON)

These examples are sufficient to show the effects of various appendages on the effective inertia ratios. Table 1 contains the effective inertia ratios computed using Eqs. (49) and (50), those computed using equations provided by Hubert[§] based on Meirovitch[2] (labeled "Ref" in Table 1), and those computed using simulation results using Eq. (74). The angle between the angular momentum vector and the probe Z-axis (i.e., the principal axis (PA) offset) and center of mass lateral offset form the central body Z-axis (CM) were also included in Table 1.

Table 1: Inertia Ratios and PA and CM Offsets at 25 RPM

Configuration	Effective Inertia Ratio					PA (deg)	CM (in)
	Eqs. (49) and (50)		Ref		Sim		
	A	β	α	β			
SBN	1.3	1.6	1.3	1.6	N/A	0	0
MBN	1.5	1.6	1.9	1.9	1.6	0	0
MBON	1.3	1.7	1.5	2.1	1.3	0.35	2.1

In general, the simulation results agreed with the analytical calculations and the results from Eqs. (49) and (50) were more conservative than results using equations from Hubert. Radial and axial boom lengths were chosen conservatively to increase stability (i.e., the effective inertia ratio) of the system relative to the probe with only magnetometer booms deployed (MBN vs. SBN). Eliminating one radial boom reduced the effective inertia ratios and moved the center of mass away from the missing boom location (MBON vs. MBN).

Having a probe Z-axis to spin axis offset does not mean the system is unstable. It means the aggregate system maximum inertia axis is at an angle with respect to the probe Z-axis. The effective inertia ratio greater than 1 indicates stability of that configuration.

RESULTS

The following sections contain a summary of THEMIS stability analyses. To ensure adequate margin, the inertia ratio was required to be greater than 1.04 for all feasible nominal and off-nominal configurations with one boom deployment failure. A principal axis offset less than 1 degree and center of mass offset less than 0.18 inch were also required in the fully deployed configuration. The probe was spin balanced to achieve principal axis offset less than 1 degree and center of mass offset less than 0.18 inch with both magnetometer booms deployed. Therefore, because the two magnetometer booms had different mass properties, the stowed configuration and configurations with one magnetometer boom deployed and the other stowed had a significant principal axis offset.

Single Rigid Body

Inertia ratios for nominal single rigid body configurations exceeded 1.34. The stowed configuration had a 10.6 degree principal axis offset and a 0.01 inch center of mass offset. Inertia ratios of the off-nominal single rigid body configurations exceeded 1.33. The off-nominal configurations with one magnetometer boom deployed and the other stowed had principal axis offsets up to 13.1 degrees and center of mass offsets up to 0.021 inches.

[§] Hubert, C., "Calculating an Effective Inertia Ratio for THEMIS," Hubert Astronautics memorandum B4024

Coupled Multi-Rigid Body

Inertia ratios for nominal multi-rigid body configurations exceeded 1.50. Given perfect alignment of the axial boom, the simulated principal axis and center of mass offsets were negligible. Inertia ratios for the off-nominal multi-rigid body configurations exceeded 1.30. However, off-nominal configurations with one magnetometer boom deployed and the other stowed had principal axis offsets up to 9.2 degrees and center of mass offsets up to 2.03 inches.

Coupled Multi-Rigid Body Sensitivity

Increasing the axial boom main stacer length by up to 0.6 meters reduced the effective inertia ratio from 1.51 to 1.19 for the deployed configuration and from 1.30 to less than 1.0 for the +Y radial boom failed configuration. The principal axis offset remained less than 1 degree for increases up to 0.3 meters. Increasing the axial boom length had a negligible effect on the center of mass offset.

Increasing the central body X-axis inertia (I_{xx}) by up to 3 kg-m^2 reduced the effective inertia ratio from 1.51 to 1.19 for the deployed configuration and from 1.30 to 1.24 for the +Y radial boom failed configuration. Increasing the central body X-axis inertia had a negligible effect on the principal axis and center of mass offsets.

Increasing the central body Y-axis inertia (I_{yy}) by up to 3 kg-m^2 reduced the effective inertia ratio from 1.51 to 1.17 for the deployed configuration and from 1.30 to 1.01 for the +Y radial boom failed configuration. Increasing the central body Y-axis inertia more than 1.5 kg-m^2 resulted in a principal axis offset greater than 1 degree. Changing the central body Y-axis inertia had a negligible effect on the center of mass offset.

Decreasing the central body spin axis inertia (I_{zz}) by up to 3 kg-m^2 reduced the effective inertia ratio from 1.51 to 1.22 for the deployed configuration and from 1.30 to 1.02 for the +Y radial boom failed configuration. Decreasing the central body spin axis inertia more than 1.5 kg-m^2 resulted in a principal axis offset greater than 1 degree. Changing the central body spin axis inertia had a negligible effect on the center of mass offset.

Decreasing the radial boom inner section length by up to 3.0 meters reduced the effective inertia ratio from 1.51 to 1.43 for the deployed configuration and from 1.30 to 1.26 for the +Y radial boom failed configuration. Decreasing the radial boom length had a negligible effect on the principal axis offset and reduced the center of mass offset by about 10%.

Simultaneously changing the axial boom main stacer length, central body axial and transverse axis inertias, and radial boom inner section length by up to 6% reduced the effective inertia ratio from 1.51 to 1.36 for the deployed configuration and from 1.30 to 1.19 for the +Y radial boom failed configuration. These changes increased the principal axis offset from 0.34 to 0.56 degrees while having a negligible effect on the center of mass offset.

SUMMARY AND CONCLUSIONS

Analytical effective inertia ratio stability criteria were derived for application to the THEMIS spacecraft (probes). The results apply to a spinning central body with flexible radial and axial booms. The central body can have unequal transverse inertias, non-zero products of inertia, and offset of the radial booms from the center of mass Z location.

Analytical and simulation-based effective inertia ratios were computed for radial and axial boom sizing and final design verification. The final THEMIS probe design was shown to be stable for sufficiently large uncertainty in mass properties to finalize the radial and axial boom designs.

ACKNOWLEDGMENTS

David Pankow, University of California at Berkeley, provided the starting point for this work through his unpublished manuscript entitled “SMEX/FAST Spin Axis Stability Discussion and Review,” and helpful feedback during THEMIS reviews. Jinho Kim and Dongyu Fu, Swales Aerospace, developed the multi-rigid body Simulink models used for simulations. Darrell Zimbelman, NASA Goddard Space Flight Center, provided FAST spacecraft hi-fidelity simulation results for Simulink model verification. Kenneth London, Swales Aerospace, assisted with the MSC.ADAMS validation simulations. Carl Hubert, Hubert Aeronautics, recommended computing the effective inertia ratio from simulation results.

REFERENCES

1. Crist, S.A. and Eisley, J.G., “Motion and Stability of a Spinning Spring-Mass System in Orbit,” Journal of Spacecraft and Rockets, Vol. 6, No. 7, July 1969, pp. 819-824.
2. Meirovitch, L., “Bounds on the Extension of Antennas for Stable Spinning Satellites,” Journal of Spacecraft and Rockets, Vol. 11, No. 3, March 1974, pp. 202-204.

3. Barbera, F.J. and Likins, P., "Liapunov Stability Analysis of Spinning Flexible Spacecraft," AIAA Journal, Vol. 11, No. 4, April 1973, pp. 457-466.

4. Meirovitch, L. and Calico, R.A., "Stability of Motion of Force-Free Spinning Satellites with Flexible Appendages," Journal of Spacecraft and Rockets, Vol. 9, No. 4, April 1972, pp. 237-245.

5. Meirovitch, L. and Calico, R.A., "A Comparative Study of Stability Methods for Flexible Satellites," AIAA Journal, Vol. 11, No. 1, January 1973, pp. 91-98.

6. Meirovitch, L. and Nelson, H.D., "On the High-Spin Motion of a Satellite Containing Elastic Parts," Journal of Spacecraft and Rockets, Vol. 3, No. 11, November 1966, pp. 1597-1602.

7. Meirovitch, L., "Stability of a Spinning Body Containing Elastic Parts via Liapunov's Direct Method," AIAA Journal, Vol. 8, No. 7, July 1970, pp. 1193-1200.

8. Dong, W.N. and Schlack, A.L., "Stability of a Spinning Satellite with Flexible Antennas," AIAA Journal, Vol. 12, No. 12, December 1974, pp. 1737-1739.